ZIBELINE INTERNATIONAL™ PUBLISHING

Water Conservation and Management (WCM)

DOI: http://doi.org/10.26480/wcm.01.2026.25.31

ISSN: 2523-5664 (Print)
ISSN: 2523-5672 (Online)
CODEN: WCMABD

RESEARCH ARTICLE

OPTIMIZATION OF THE TECHNICAL SOLUTION FOR AN EXPANDING STILLING DEVICE BEHIND A CULVERT

Olga Chernykh[a], Nartmir Khanov[a], Bakhodir Norkulov[b, c]*

[a]Russian State Agrarian University – Moscow Timiryazev Agricultural Academy, Moscow, Russian Federation
[b]Samarkand State Architecture and Construction Institute, Samarkand, Uzbekistan
[c]"Tashkent Institute of Irrigation and Agricultural Mechanization Engineers" National Research University, Tashkent, Uzbekistan
**Corresponding Author Email : vohidov.oybek@bk.ru, norqulov.baxodir@samdaqu.edu.uz*

Article History:

Received 11 September 2025
Revised 25 November 2025
Accepted 30 December 2025
Available online 21 January 2026

ABSTRACT

The key aspect of this study is the recommendations for prediction of pulsation loads and calculation of slabs of the drainage basin with energy-absorbing elements of a cavitation-resistant structure. Using computational analysis and hydrodynamic studies, the configuration of the basin was selected, which had not previously been encountered in the operated devices of the downstream of irrigation hydraulic structures. Optimization of the structural elements of the expanding spillway head will ensure reliable operation of the branch channel during the implementation of the modernized preliminary project. This ensures stable flow in the outlet channel below the spillway apron regardless of the stage of cavitation or changes in the spectrum and magnitude of pressure pulsations in individual attachment points and local sections of the damping pool.

KEYWORDS

Low-span spillway, energy dissipators, anti-cavitation protection, expanding stilling basin, flow disruption, pressure and load pulsation, slabs.

1. INTRODUCTION

The Lower Kafirnigan hydrotechnical complex is an important facility for Tajikistan. It is designed taking into account seasonal regulation of the reservoir volume of at least 2.05 km ^{3}, the projected annual electricity generation of 0.6 billion kWh. Conceptual design for this irrigation waterworks began in the 1980s. The designated irrigation zone covers approximately 146,200 hectares of arable land suitable for irrigation, of which only 42,700 hectares are currently irrigated. All construction work begun for a number of reasons was discontinued in 1992.

The Kafirnigan river - right tributary of the Amu Darya River in Figure 1 originates from the southern slopes of the Gissar Range. The river extends 387 km with a basin area of 11,600 km^2 and mean discharge of 156 m^3/s.

Figure 1: Hydraulic complex construction site and deteriorated settlement infrastructure adjacent to the Kafirnigan River hydroelectric development project, originally established in 1983 (Photo: Asia-Plus, 2024).

Quick Response Code	Access this article online	
	Website: www.watconman.org	**DOI:** 10.26480/wcm.01.2026.25.31

Cite The Article: Olga Chernykh, Nartmir Khanov, Bakhodir Norkulov (2026). Optimization of The Technical Solution For an Expanding Stilling Device Behind a Culvert. Water Conservation and Management, 10(1): 25-31.

The flood control complex comprises a 1,600 m long dam made of locally produced material with an asphalt concrete lining, a bottom pipe spillway, an irrigation outlet, an emergency spillway (capacity 650 m^3/s), and an 80 MW hydroelectric power station with an average annual output of 478,000 kWh. The spillway comprises a 70 m high tower, lock chambers, and four 230 m pipes with a design flow rate of 1,290 m^3/s. The terminal section consists of a four-span pipe discharging into a flared stilling basin with a central angle of 20° (Rozanov et al., 1979; Rozanov et al., 1984; Obidov et al., 2020; Bazarov et al., 2021). Preliminary studies have shown inadequate energy dissipation and flow distribution in the tailrace during operational and flood releases (Omarova et al., 2025 ; Rozanova and Ariel, 1983).

Over the past three decades, significant progress has been made in research dedicated to optimizing the protection configurations of tailraces in both open and closed (tubular) spillway systems, ensuring the effective dissipation of excess flow energy. Research shows that virtually no tailrace configuration in short-span tubular hydraulic structures provides satisfactory energy dissipation and flow distribution without the implementation of combined systems of energy absorbers, flow dividers, and distributors arranged in several consecutive rows (Rozanov et al., 1984).

2. Materials And Research Methods

Hydraulic investigations of the preliminary design were conducted in the laboratory complex of the Department of Hydraulic Structures of the A.N. Kostyakov Institute of Amelioration, Water Management, and Construction (Burlachenko et al., 2024).

Primary studies used a three-dimensional hydraulic model of the Lower Kafirnigan spillway design at 1:60 linear scale in Figure 2 (Chernykh et al., 2023 ; Chernykh and Komelkov, 1983). Expected flow velocities upstream of the first dissipator row could exceed 24 m/s, indicating potential cavitation inception capable of damaging dissipator surfaces during operation. Various "erosion-free" dissipator-distributor and threshold-wall configurations were examined. Cavitation conditions in energy dissipator zones were analyzed using fragment model data from vacuum testing facilities (works under the direction of Prof. Dr. N.P. Rozanov, A.G. Zhuravleva, A.R. Ariel and B.M. Obidov). The main parameters of the stand are given in (Rozanov et al., 1984). Hydraulic and hydrodynamic investigations of the stilling basin and discharge channel occurred at Froude numbers $Fr_1 = V_1^2/gh_1$ ranging from 51 to 190 and Reynolds numbers from 412,000 to 527,000, calculated for a contracted cross section with depth h_1 and acceleration of gravity g = 9.81m/s².

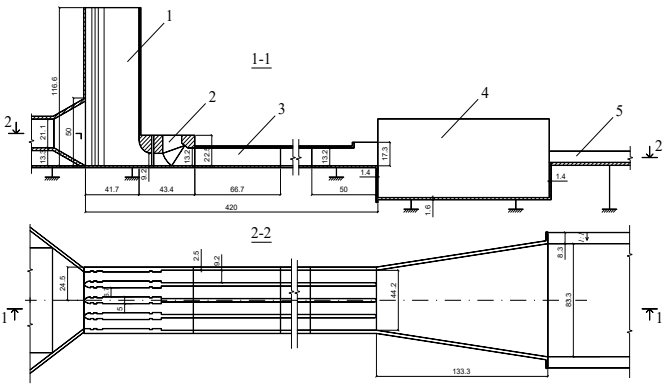

Figure 2: Schematic diagram of the four-span tubular spillway hydraulic model for the Kafirnigan River hydroelectric complex: 1 - intake tower; 2 - gate chamber; 3 - conduits, $i = 0.0175$; 4 - stilling basin; 5 - discharge channel (model dimensions in centimeters)

During the hydrodynamic experiments, pulsation pressures were measured at 30 distinct points along the length of the stilling basin. The experiment used inductive point pressure sensors of the membrane type, with a diameter of 6 mm, designed to withstand a maximum pressure of 30 cm H_2O in Figure 3. The experiment also employed a tested block diagram of control and measuring equipment, accompanied by appropriate software. The static pressure component was measured at 42 points using piezometers. The frequency and amplitude characteristics were expressed numerically within the prescribed ranges. For the frequency range from 0.2 Hz, the spectral densities were recorded with an error of less than 2 dB. The root mean square (RMS) error of the measurements was 4%.

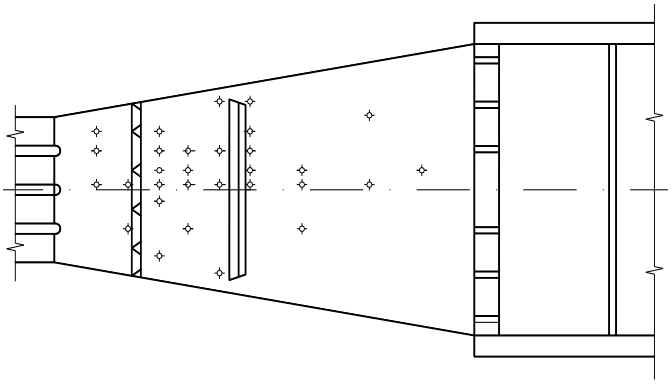

Figure 3: Spatial distribution of DDM-6 pressure sensors on the stilling basin floor with the optimized energy dissipation system configuration.

The cases for which the research was conducted are enumerated in Table 1.

Table 1: Calculated modes and parameters

Case №	Case name	Flow rate, m^3/c	Water level mark of the upper bank, m	Number and location of operating orifices (pipes)
1	Construction	1240	472.7	
2	1st operational	1290	505	
3	2nd operational	1290	525	
4	2nd operational	1080	525	
5	2nd operational	720	525	
6	2nd operational	720	525	
7	2nd operational	360	525	
8	2nd operational	360	525	

Six stilling basin designs were evaluated, in which the first-row dissipators had erosion-resistant profiles, often serving as flow distributors. The basin depth, dissipator configuration, and flow distributor sizes varied. The smooth-bottom variant was immediately rejected due to unsatisfactory flow distribution during three-tube operation (Case No. 4).

3. Results And Discussion

3.1 Experimental studies of the well design

Studies have shown that efficient energy dissipation, proper flow distribution and trouble-free operation under all operational discharge scenarios (symmetrical and asymmetrical) can be achieved through certain structural measures:

- Installation, along each of the four span axes, of triangular erosion-

resistant flow distributors with inclined upper faces (slope 1:2.3), positioned 15 meters downstream from the beginning of the basin. Their lower faces rest on anti-cavitation thresholds (not exceeding 0.3 m in height) constructed with a reverse slope.

- Placing a dispersing threshold at a distance of 33 meters from the beginning of the stilling basin, while all flow surfaces, with the exception of the frontal one, are made in the form of inclined surfaces (slope 1:2.3) to increase anti-cavitation protection, with lateral anti-cavitation thresholds (maximum height 2.8 m).
- Installation of six flow dividers (2 m high, 1 m thick) at the outlet edge of the stilling well.
- Placing an additional stilling basin (0.9 m height) on the apron 30 meters downstream of splitters.

This combined solution improved flow width distribution, stabilization, and dissipation system effectiveness beyond the terminal protection section. Laboratory design and subsequent experimental verification produced the tailrace protection configuration shown in the study Figure 4. The tailrace connection in this protection system uses three hydraulic jumps: the first is above the triangular distributors, the second is at the end of the pool after the distribution threshold, and the third is between the outlet edge of the pool and a small stilling wall.

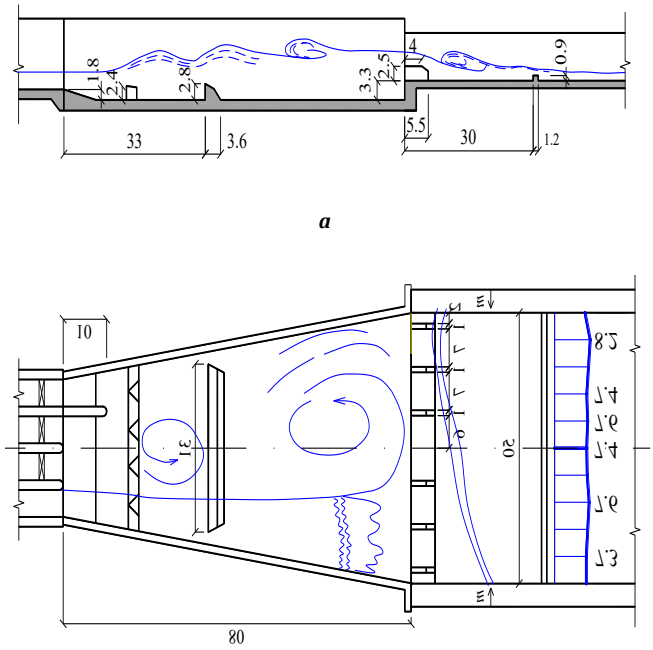

Figure 4: Longitudinal profile along the centerline of the discharge section (a) and plan view of flow patterns at the spillway with velocity distribution on the stilling basin apron (b) during single left conduit operation (Case No. 8)

Mean pressure and flow loading were determined by piezometric line height above stilling basin bottom elevation. All operational cases exhibited identical pressure distribution along protection: pressure increase upstream of dissipators, sharp decrease downstream, then renewed increase before solid walls. Maximum differential occurred during power plant tube closure with three adjacent tubes operating, reaching 0.55 ($\rho V_1^2/2$), or 16.6 m H_2O in prototype conditions (ρ - density of water, t.s^2/m^4, V_1 - velocity at the pipe outlet).

Pressure upstream of solid walls exceeded tailwater depth, averaging 0.46($\rho V_1^2/2$). From solid wall to perforated threshold wall, piezometric levels remained essentially constant at (0.23...0.27) ($\rho V_1^2/2$). Downstream of perforated walls in the third roller zone, local pressure reduction occurred, corresponding to tailwater levels over relative length l/h_1 = 25 (h_1 representing the depth at the pipe outlet).

The pressure distribution across the channel width during symmetrical span operation exhibits relatively uniform characteristics. Under asymmetrical operational conditions, the most pronounced non-uniform distribution occurs upstream of the first row of energy dissipators, while downstream of these elements, the pressure distribution becomes more uniform, achieving a nearly horizontal profile.

Regions of reduced pressure encompass the first row of stilling basin slabs, where the initial slab experiences alternating loading conditions, and extend into the upstream sections of the second row of slabs. Assuming sub-slab pressure equals tailwater pressure, the maximum pressure deficits under design operational conditions will affect slabs positioned downstream of the first and second rows of energy dissipators. During partial span operation of the structure, flow separation occurs downstream of the first and second row dissipators, resulting in redistribution of mean pressure values. The maximum pressure deficit is observed along the centerline of the separated flow within the jet impingement zone. Localized pressure increases appear at the opposite channel boundary, reaching magnitudes of 10…15 m water column during two-span operation (Cases No. 5 and No. 6) or three-span operation (Cases No. 7 and No. 8). Upstream of the third row of energy dissipators, both pressure and velocity distributions become equalized.

3.2 Cavitation studies

Since prototype cavitation conditions reduce the drag coefficients of first-row energy dissipators C compared to conventional hydraulic model testing (as opposed to vacuum chamber testing considered in previous studies (Obidov et al., 2020). One of the most feasible approaches was employed to estimate total loading magnitudes: cavitating energy dissipators under full-scale conditions were replaced by geometrically similar dissipators with reduced midship cross-sectional areas ω by a factor of C_0/C_k, where C_0 and C_k represent drag coefficients for non-cavitating conditions ($\beta > 1$) and specified cavitation stages ($\beta = K/K_{cr}$ where K is the cavitation parameter calculated based on model studies at V_n - the flow rate at the height of the damper, K_{cr} = 0.8 - the critical cavitation parameter determined in a cavitation stand), respectively. The coefficient C is derived from the established formula for energy dissipator reaction assessment: $R = \gamma\omega CV^2_n/2g$, where commonly accepted values are utilized (Lappo, 1998 ; Hydraulic engineering structures (spillway, outlet and culverts). 2016. Design rules. Code of Rules. SP 290. 1325800.).

When implementing this methodology, simultaneous experiments were conducted using first-row energy dissipators with both reduced and original cross-sectional areas to verify that cross-sectional modifications did not significantly influence flow structure characteristics. The obtained drag coefficient values C_0 for the investigated energy dissipators demonstrate excellent agreement with data presented in previous research (Chanson, 2015 ; Chernykh et al., 2023). Investigations were conducted using sensor plate technology that enabled determination of both dissipator reactions and load pulsation coefficients (Alsadek, 2024 ; Kumar et al., 2000). Experimental results demonstrate that load pulsation coefficients increase progressively with cavitation development in Figure 5, while at $\beta < 0.5$, a tendency toward coefficient reduction emerges, consistent with expectations based on investigations by (Rozanova and Ariel, 1983).

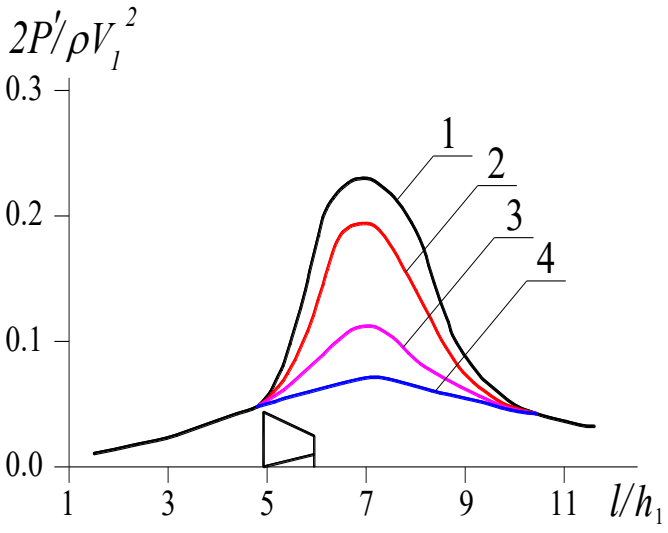

Figure 5: Streamwise distribution of normalized pressure fluctuation standards ($2P'/\rho V_1^2$) on the stilling basin floor behind erosion-free first-row energy dissipators as a function of relative distance (l/h_1) for different cavitation parameters β: 1 - β = 0.5; 2 - β = 0.7; 3 - $\beta > 1$ (no cavitation); 4 - β = 0.2

The effect of cavitation stage β on the load change factor δ_n is shown in Figure 6. When energy dissipators work under cavitation conditions, both starting and growing stages, the instant load parts increase (while the average load decreases) compared to flow without cavitation. Under non-cavitating conditions, the load change factor δ_n was found as $\delta_n = \pm A/(V^2/2g)$, where A denotes the load variation normalized by the cross-sectional area ω, and $V_1^2/2g$ is the velocity head from approach flow speed to the energy dissipator. This factor stays constant at δ_n = 0.061...0.11 for erosion-free energy dissipators in the first row.

At the early stage of cavitation, this value grows and reaches δ_n = 0.65 when β = 0.5 in Figure 6. The growth of the change factor relates to the formation of a natural disturbance center - a cavitation plume containing many collapsing and vibrating bubbles. The decrease of changes at some cavitation stage, due to a "cavitation threshold" that stops absolute pressure from dropping below liquid vapor pressure, was noted earlier by V.M. Lyatkher (Obidov et al., 2020).

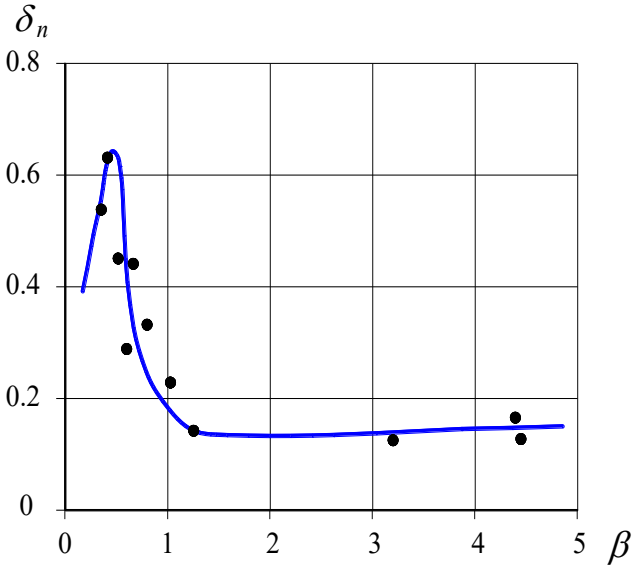

Figure 6: Relationship between load pulsation coefficient and cavitation parameter ($\delta_n = f(\beta)$) for erosion-resistant energy dissipator designs

3.3 Hydrodynamic effect on plates

The satisfactory operation of the stilling basin for the four-span tubular spillway of the Lower Kafirnigan irrigation complex required special conditions across a wide range of heads (construction and operational cases) and during gate operations (any combinations of open and closed spans). The distribution of pressure pulsation intensity P' in the section upstream of the first row of energy dissipators closely matches known experimental data for hydraulic jumps. The value of P' here is approximately 0.06($\rho V_1^2/2$), except for single-tube operation modes (Cases No. 7 and No. 8), which is explained by sharp decreases in specific discharge rates and velocities in the contracted section.

The highest values of P' are observed downstream of the first row of energy dissipators (erosion-resistant blocks) at distances of (0.55...1.0)h_1 and reach 0.2($\rho V_1^2/2$) during construction periods and 0.145($\rho V_1^2/2$) during operational periods in the same cross-section. The maximum value of P' occurs in the jet impingement zone when only the two middle spillway tubes operate (Case No. 6), reaching 0.245($\rho V_1^2/2$). In the region between the first and second rows of energy dissipators, pressure pulsation values range from 0.2 to 0.04($\rho V_1^2/2$), which is slightly higher than conventional data for hydraulic jumps (Chanson, 2015 ; Bazarov et al., 2025). This is due to three-dimensional flow effects and the fact that velocity in the contracted section differs from velocity at tube exits. The large P' values downstream of flow distributors result from three-dimensional flow separation around the blocks, creating intense vortex formation behind them. As flow approaches the solid wall, pulsation intensity decreases to 0.04($\rho V_1^2/2$), and downstream of the wall up to the perforated threshold wall, P' = 0.03($\rho V_1^2/2$), with slower decay rates in Figure 7.

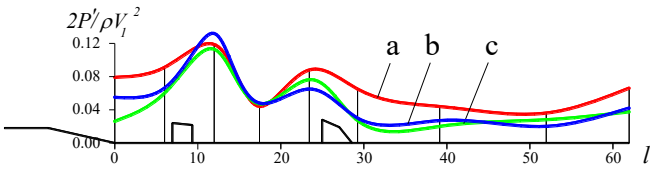

Figure 7: Distribution of relative pressure pulsation standards at stilling basin floor measurement points $2P'/(\rho V_1^2/2)$ during design discharge Q = 1290 m^3/s with all four tubes operating: longitudinal section between first-row erosion-resistant energy dissipators (a), hydraulic jump reference data (b), and along energy dissipator centerline (c)

Correlations between the sensor installed at the center of the first slab and the remaining sensors were evaluated on the model considering the preliminary division of stilling basin slabs (Figure 8). Despite the fact that pulsation standard values in some cases were significant - exceeding 0.1($\rho V_1^2/2$), where V_1 can be taken as the velocity in the section at the stilling basin entrance (or at the tube outlets in the case of a tubular spillway, practically for all considered operational modes the correlation was either small or completely absent (Usanova et al., 2025 ; Rubin et al., 2025). This indicates intensive averaging (mixing) processes, especially across the flow direction. Even for nearby sensors in Case No. 1, the correlation is negative, which is explained by the presence of intermediate disturbance sources. The turbulence here is clearly three-dimensional and the spatial correlation has an asymmetric shape. Along the flow direction, correlation changes less sharply than across the flow in Figure 8a.

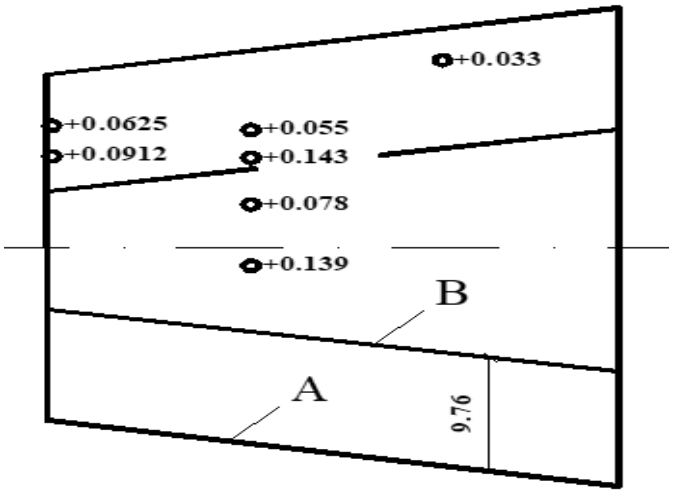

A

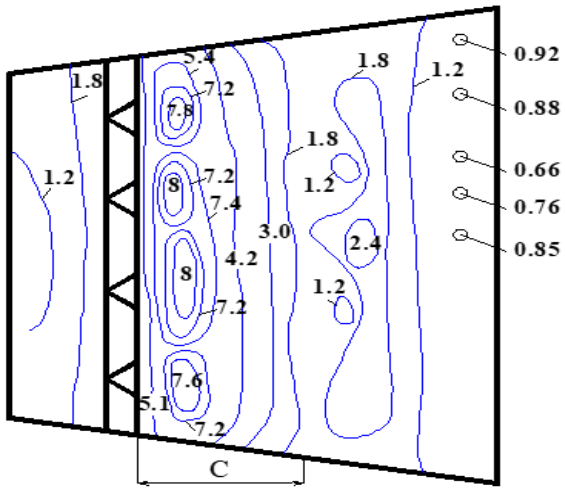

b

Figure 8: Calculation schemes for determining loads on first-row slabs with energy dissipators in the irrigation hydraulic complex stilling basin: (a) correlation coefficient values at slab measurement points divided into structural zones A and B (correlation coefficients r_{ij} = 0 at remaining points); (b) pressure pulsation standard contour lines P' considering cavitation effects in zone C (in meters water column at prototype scale)

The central portion of the first-row slab experiences maximum loading during construction period operations. When the structure operates with three spans (Case No. 4), the area with maximum P' values shifts toward the span axis adjacent to the closed opening. In this case, P'_{max} = $0.16(\rho V_1^2/2)$, while downstream of the solid wall, P' values decrease to $0.03\rho V_1^2/2$. Pressure pulsation standard data processed to obtain contour lines in Figure 8 also showed that concentration of P' values occurs in the middle portion of the first slab downstream of flow distributors, with P' values decreasing near the channel sides. Upstream of the solid wall in some operational modes, local areas with increased P' values still exist. Zero values of pressure correlation coefficients were also observed at these locations in Figure 8a. For this case, the pulsation loads were determined using the NIS Hydroproject methodology (Rozanov et al., 1979). When creating calculation matrices, two cases of stilling basin division into slabs were considered: Case A - the first slab occupies the entire area between vertical walls; Case B - the slab occupies only the central portion (corresponding to the preliminary design division of the stilling basin into slabs). In Case A, the first-row slab ($L \times L$ = 32×32 m) was divided into 8 elementary square areas with dimensions $L_0 \times L_0$ = 4×4 m. In Case B, the 32×16 m slab was also divided into 4×4 m squares. For each elementary square, the averaging coefficient was calculated using the formula:

$$K_0 = \frac{P_0'^2}{P'^2} = 0.55 + 0.45 r_{ij} \quad (1)$$

$$P_0 = K_0^{0.5} \cdot P' \quad (2)$$

where $P_o'^2$ represents the variance of specific load fluctuations on area $L_0 \times L_0 = \Omega_0$; P'^2 is the mean variance value of fluctuations at measurement points determined along lines of equal standards; r_{ij} – is the mutual correlation coefficient between points at the centers of elementary areas.

The pulsation standards of specific load P_p' and load equivalent to specific overturning moment action P_m' were determined according to relationships tested in previous studies (Rozanov et al., 1984; Chernykh et al., 2025):

$$P'_p = \Omega_0/\Omega \cdot (\Sigma P'^2_{oi} + 2\Sigma\Sigma P'_{oi} \cdot P'_{oj} \cdot r_{jo})^{0.5} \quad (3)$$

$$P'_m = \Omega_0/\Omega \cdot 2/L \cdot (\Sigma P'^2_{oi} \cdot X_i^2 + 2\Sigma\Sigma P'_{oi} \cdot X_i \cdot P'_{oj} \cdot X_j \cdot r_{ijo})^{0.5} \quad (4)$$

where n is the number of elementary areas; X_i and X_j – are distances from centers of elementary areas to the reference edge for moment calculation (downstream edge of first-row slab); r_{ijo} – is the correlation coefficient between pulsation loads applied to elementary areas.

Since correlation values are very small in Figure 8a or even negative, it was assumed that $r_{ijo} = r_{(ij)}/K_o$ approaches zero. This leads to a conservative design approach. Load standard calculations for the first-row slab yielded: Case A – P'_p= 0.172 t/m², P'_M = 0.214 t/m²; Case B – P'_p = 0.276 t/m², P'_M = 0.31 t/m². These results show that the load equivalent to overturning moment action determines slab thickness requirements.

To estimate maximum pulsation load amplitude on slabs, transition coefficient K_A was determined for converting from root-mean-square values to maximum deviations occurring with specified probability p_o during design flood passage time T:

$$K_A = \sqrt{2ln\frac{T/\tau_0}{2\ln(1/p_0)}}, \quad (5)$$

where the characteristic pulsation period is:

$$\tau_0 = \pi \sqrt{\frac{\int_0^\infty S_p(\omega)d\omega}{\int_0^\infty \omega^2 S_p(\omega)d\omega}}. \quad (6)$$

Adopting T/τ_o = 10^6 and p_o = 0.95 for Class 1 responsibility structures yields K_A = 5.67 (maximum possible value) [1,4]. The extreme specific load equivalent to overturning moment action for the first-row slab equals: Case A – $P'_{M\,(max)} = K_A P'_M$ = 5.67·0.12 = 1.21 t/m²; Case B – $P'_{M\,(max)}$= 5.67·0.31 = 1.76 t/m².

The expediency of dividing the Nizhne-Kafirnigansky spillway into 2 40 m long slabs along its length has been experimentally proven in Figure 9. The support slabs can be either undrained or drained. In the latter case, it is recommended to arrange drainage wells directly behind the first row of energy absorbers – at a distance of 1.5...2.5 m from the downstream edge of the spreaders. It is desirable to have 2 rows of drainage wells, the distance between individual wells being 7...10 m. The number of drainage wells is determined by filtration calculations. To protect against possible dynamic effects of the flow, the inlet openings of the drainage wells must be covered with a specially designed lid (Sinha et al., 2025; Prosekov et al., 2022).

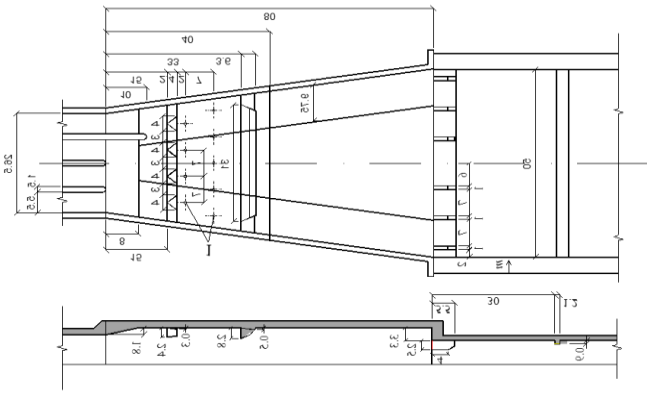

Figure 9: Recommended option for the renovation of the design solution for the execution of a stilling area with the placement of drainage wells (1) of a special design (conditional marks and dimensions are given in m)

Second-row slabs typically positioned downstream of subsequent energy dissipator rows, such as those located downstream of solid walls (as implemented in the Lower Kafirnigan, Podolsk, Shamkir, Kursk multipurpose hydraulic complexes and other projects investigated using this methodology, experience minimal pulsation effects (Burlachenko, 2024 ; Chernykh et al., 2025). This occurs because the jet trajectory over the wall, even when perforated, typically impacts a substantial water depth that dampens jet action on the stilling basin floor.

Investigation results demonstrate that for similar low-span structures operating under emergency conditions, pulsation standard values on first and second-row slabs are lower than during design operational modes. Therefore, slab thickness determination should be based on primary operational conditions when maximum discharge passes through all spans (for example, in the Lower Kafirnigan hydraulic complex during four-tube operation in Case No. 3: Q = 1290 m³/s and upstream water level = 525 m).

To increase slab stability or reduce slab thickness requirements when necessary, specialized drainage wells can be installed at locations of maximum pressure reduction: downstream of first-row energy dissipators at distances of (1...2)h_1, and downstream of second-row energy dissipators at distance $0.5h_1$.These drainage systems should incorporate pulsation-stabilizing designs that regulate pressure fluctuation transmission to sub-slab areas.

For evaluating local strength of stilling basin slabs, three key cases of probable extreme loading should be considered for design load determination: maximum P' located above the first row of drainage openings commonly constructed in stilling basins for pressure relief minimum and maximum values at the downstream edge of slabs along the flow direction.

The load acting on each section P_j is expressed as:

$$P_j = \bar{P}_j + P'_j \quad (7)$$

The mean load distribution $\bar{P}_j$ can be constructed from experimental data. When maximum deviation from mean value P'_{jmax} occurs at one slab section, the most probable value at other sections equals the local maximum deviation multiplied by the spatial correlation coefficient between considered sections:

$$P'_j = P'_{jmax} \cdot r_{ij} \quad (8)$$

Thus, by calculating P'_j values according to longitudinal and transverse correlations, the loading field can be constructed to identify the most

critical loading conditions. Calculations must also account for local increases in hydrodynamic loading, particularly in areas where erosion-resistant energy dissipators are installed (Chernykh et al., 2024).

3.4 Assessment of the thickness of the mounting plates

Local strength assessment of protection slabs may reveal situations where slab thickness determined by stability calculations with allowable reinforcement does not provide adequate local strength; in such cases, slab thickness must be increased. Verification of the calculation methodology for Cases A and B was performed using experimental data and relationships (1) – (8) for the Lower Kafirnigan hydraulic complex outlet section, with representative results presented in Figure 10. Calculations are performed per linear meter of slab width (Chernykh et al., 2025).

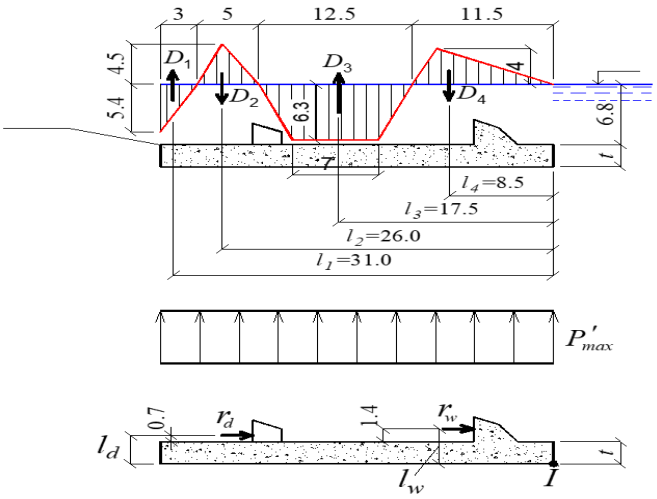

Figure 10: Design calculation schemes for load determination on first-row stilling basin slabs with erosion-resistant energy dissipators during full spillway operation with all spans (Case No. 3)

Based on hydraulic and hydrodynamic investigation results, when the first-row slab occupies the entire stilling basin area (Case A), its thickness t can be determined from overturning stability conditions without stilling basin drainage using the following formula:

$$t = \{P'_{m.max} + \Sigma D_i \cdot l_i/0.5L^2 + \Sigma r_i \cdot l_{ri}/0.5L^2\} \cdot \{K_3/(\gamma_c - \gamma_w)\} \quad (9)$$

where D_i· and l_i represent pressure deficits and moment arms of these forces according to the mean pressure distribution in Figure 10; r_i are horizontal loads on energy dissipator-distributors and walls; l_{ri} are moment arms of these forces relative to point O; γ_c and γ_w – are specific weights of concrete and water, respectively (Sidorova, 2022 ; Markova et al., 2025 ; Yu et al., 2025).

For this structural configuration:

$$\Sigma r_i \cdot l_{ri} = \left(\bar{R}_\gamma \cdot 4 \cdot l_g/B_{v1}\right) + \left(\bar{R}_{st} \cdot l_{st}/B_{v2}\right) \quad (10)$$

$$\bar{R}_\gamma = \gamma_w \cdot \omega_g \cdot C_\gamma \cdot V_n^2/2g \quad (11)$$

where: ω_g – is the vertical face area of one energy dissipator above the sill; C_γ = 0.5 is the dissipator drag coefficient under design conditions accounting for cavitation stage at β = 0.5 in Figure 6; V_n = 23.3 m/s is the mean approach flow velocity at dissipator top level, measured on the model; B_v is the stilling basin width at the location of the considered flow energy dissipator; K_3 = 1.05 is the safety factor; l_γ and l_{ri} are moment arms of forces $\bar{R}_\gamma$ relative to point O.

Substituting all specified values into formula (9) for spillway operation with all spans fully open in Case No. 3, the minimum thickness of protection slabs for the transition section was obtained. For the first row of stilling basin protection, which experiences the greatest hydrodynamic loading, results for optimal thickness assessment ensuring reliable and safe operation of the entire tailwater are presented in Table 2.

Table 2: Design thickness specifications for energy dissipation basin slabs in the low-span spillway system of the irrigation hydraulic complex, t (m)

Stilling basin slab configuration	Without stilling basin drainage		With stilling basin drainage	
	Without cavitation	Including cavitation	Without cavitation	Including cavitation
First-row slab occupies entire basin floor area (Case A)	1.9	2.6	1.07	1.71
First-row slab occupies only central portion of area (Case B)	2.4	3.26	1.5	2.36

When installing drainage openings according to developed recommendations for each structural configuration of energy dissipation devices, pressure fluctuation above drainage openings must be considered. By representing pressure pulsation spectrally using Fourier transformation from the system of equations describing slab motion before uplift, spectral densities, standards, and covariances of hydrodynamic flow effects can be obtained. This approach enables assessment of expected slab displacements $u_0(t)$ (slab uplift), probability of reverse filter reformation beneath drainage openings and slabs under natural composition conditions, and analysis of overall slab-foundation system stability. Alternatively, specialized drainage well designs can be implemented to restrict pressure pulsation penetration beneath slabs.

4. Conclusions

The resumption of the construction of a hydroelectric power station on the Kafirnigan River will improve irrigation and drinking water supply in the Asian republics. As a result, irrigated lands in Tajikistan and Uzbekistan, where there is a shortage of water, will be expanded. In the future, when restoring the structure, special attention should be paid to hybrid modeling of hydrodynamic processes at the spillway using 3D models and taking into account the results obtained:

- A study of the preliminary design of a low-span spillway revealed design flaws. They significantly reduce operational reliability and increase construction costs. The erosion-free form of the dampers has been selected. A relationship has been established between a decrease in the coefficient of resistance of the spreading dampers depending on the cavitation stage. As a result, the area of the midsection of the dampers was reduced by 66%.
- The maximum pulsation components of the load on the culvert plates are observed at the stages of advanced cavitation and can exceed the load in non-cavitation operating conditions by more than 2 times. For the design mode (when all pipes are operating), the pulsation part of the load is 30% of the static one.
- The cross-section experiencing maximum pulsation loads is located behind the erosion-free energy dampers at approximately a distance of (0.5...1.5)h_1 (h_1 is the depth of the flow at the outlet of the pipes).
- With the selected dampener scheme, a low spatial correlation is observed in the area behind the 1st and 2nd row of dampers. It is characterized by fast attenuation. It is proved that the loading field must be constructed when assessing the strength and stability of slabs, necessarily taking into account local and spatial changes in the correlation of load standards. In the area of installation of erosion-free dampers, a local increase in hydrodynamic loads should also be added. The obtained graphical dependencies make it possible to optimize the layout of drainage wells on the gutter and their design. It is proposed to make at least 2 rows of slabs.

Author Contributions

Olga Chernykh: Conceptualization, Research methodology, Data curation, Data analysis, Project administration; Nartmir Khanov: Grammar and scientific writing, collecting research data, designing research equipment, testing; Bakhodir Norkulov: corresponding author, writing research drafts, editing, finalizing articles.

Acknowledgments

The study was carried out as part of the project to create and develop

the Engineering Center at the Russian State Agrarian University-Moscow Agricultural Academy named after K.A.Timiryazev (agreement No. 075-15-2025-543 dated June 16, 2025).

REFERENCES

Rozanov, N.P., Kaveshnikov, N.T., Kitov V.I., 1984. Devices of the spillway lower bank. Kolos (Moscow), Pp. 78-92.

Rozanov, N.P., Rumiantsev, J.S., Rozanova, N.N., Kaveshnikov, N.T., Kitov, E.I., Bukreiev, V.P., Chernykh, O.N., Chechonadskikh, V.S., 1979. Rational Types and Designing of Tailwater arrangements in open spillways. Spillway Tunnels and Culvert-type spillways. International Comission on Large Dams, XIII Congress, New-Delhi, India.

Obidov, B., Vokhidov, O., Shodiev, B., Ashirov, B., Sapaeva, M., 2020. Hydrodynamic loads on a water drain with cavitation quenchers. IOP Conference Series: Materials Science and Engineering, 883(1). doi:10.1088/1757-899x/883/1/012011.

Omarova, P., Neftissov, A., Kazambayev, I., Kirichenko, L., Aubakirova, A., and Borsikbayeva, A., 2025. Numerical Simulation and Verification of Free-Surface Flow Through a Porous Medium. Water, 17(24), 3505. https://doi.org/10.3390/w17243505

Rozanova, N.N., Ariel, A.R., 1983. Cavitation and hydraulic investigations of erosion less energy dampers. Collection of scientific papers. Natural and model studies of hydraulic structures. (Moscow), Pp. 75-81.

Burlachenko, A.V., Burlachenko, Y.Y., Brakeni, A., Chernykh, O.N., 2024. Ensure the stability of the water retention plates of hydraulic structure. Larhyss Journal, 58, Pp. 73- 87.

Lappo, D., 1988. Hydraulic calculations of spillway hydraulic structures: a reference guide. Energoatomizdat (Moscow), Pp. 146-193.

Chernykh, O.N., Burlachenko, A.V., Burlachenko, Ya.Yu., 2023. Experimental and analytical studies of the loads on the anchoring elements behind the spillways of the water objects of the AIC. Environmental Engineering, 4, Pp.12-20.

Chernykh, O.N., Komelkov, L.V., 1983. Hydrodynamic loads and stability of the lower-pool apron of hydraulic structures. Hydrotechnical Construction, 17(8), Pp. 410-416.

Burlachenko, A.V., Chernykh, O.N., Brakeni, A., 2023. Operation evaluation of water discharge end sections in the conditions of narrow down throw. Larhyss Journal, 56, Pp. 25-38.

Hydraulic engineering structures (spillway, outlet and culverts). 2016. Design rules. Code of Rules. SP 290. 1325800. https://docs.cntd.ru/document/456074911.

Chanson, H., 2015. Energy dissipation in hydraulic structures. CRC Press (London, UK).

Chernykh, O.N., Burlachenko, A.V., Burlachenko, Ya.Y., 2023. Ensuring the reliability of the slab fixing behind the culverts of the reclamation systems of the AIC. Environmental Engineering, 5, Pp. 41-46.

Alsadek, E.S., 2024. Fastenings in the downstream of the mine spillway of the hydroelectric complex "16 Tishrin". Environmental Engineering, 3, Pp. 63-70. https://doi.org/10.26897/1997-6011-2024-3-63-70

Bazarov, D., Vatin, N., Obidov, B., Vokhidov, O., Rakhimov, A., and Akhmadi, M., 2021. Hydrodynamic effects of the flow on the slab of the stand in the presence of cavitation. In IOP Conference Series: Materials Science and Engineering, 1030(1), doi:10.1088/1757- 99X/1030/1/012116

Kumar, P. S., Kumar, M. S., and Pandit, A. B., 2000. Experimental quantification of chemical effects of hydrodynamic cavitation. Chemical Engineering Science, 55(9), Pp. 1633-1639. https://doi.org/10.1016/S0009-2509(99)00435-2

Burlachenko, Ya.Y., 2024. Justification of dynamic loads calculation for estimation of local strength of slabs of a separate wall of a complex purpose hydrostructure. In Proceedings of the International Scientific Conference of Young Scientists and Specialists, dedicated to the 150th anniversary of A.Y. Milovich, 1, Pp.110-114.

Chernykh O.N., Burlachenko A.V., Burlachenko Ya.Yu., 2025. Hydrodynamic Studies of an Expanding Aqueous Sluice with Erosion-Free Energy Dissipators Behind a Tubular Spillway. Environmental Engineering, 4. Pp. 81-88.

Prosekov, A., Timoshchuk, I., Gorelkina, A., Golubeva, N., Ivanova, L., and Onopenko, S., 2022. Environmental monitoring in the area of the Krapivinsky hydroelectric complex during the assessment of the current state and during the construction period of HPP. In AIP Conference Proceedings, 2636(1), https://doi.org/10.1063/5.0104303

Usanova, K., Bazarov, D., and Yu, K., 2025. Effect of fly ash as partial replacement of cement on strength and workability of concrete. In AIP Conference Proceedings, 3256(1), https://doi.org/ 10.1063/5.0267488

Bazarov, D., Norkulov, B., Artikbekova, F., Mamataliev, A., Ahmadi, M., Salimbaeva, I., and Ahmadova, E., 2025. Numerical studies in the bed of the Amudarya river at the site of damless water intake into the Karshi Main Canal. In AIP Conference Proceedings, 3256(1), https://doi.org/10.1063/5.0266916

Rubin, O. D., Bazarov, D. R., Lisichkin, S. E., Frolov, K. E., and Junhaoi, Z., 2025. Calculation of reinforcement with composite materials in reinforced concrete for hydraulic structures, including those subject to uneven settlement. In AIP Conference Proceedings, 3256(1), https://doi.org/10.1063/5.0267491

Sinha, M. K., Anand, A., Kishore, K., Singh, A., Ivanovich Vatin, N., and Bazarov, D., 2025. Exploring the morphology, rheology and compressibility of aluminium saw chips and fly ash mixture during processing through powder metallurgy route. In AIP Conference Proceedings, 3286(1), https://doi.org/10.1063/5.0279306

Yu, K., Jiang, Y., Ding, Y., Ukrainczyk, N., Li, L., Kalandarbekov, I., and Zhang, Z., 2025. Rebar/Corrosion-Free HS-ECC Beam for coastal structures: Optimization for Exceptional Strength-to-Mass Ratios. Case Studies in Construction Materials, e04812. https://doi.org/ 10.1016/ j.cscm.2025.e04812

Markova, I., Khanh, P. K., Vokhidov, O., and Gadiyeva, U., 2025. Flood study in downstream of river Sai Gon-Dong Nai. In AIP Conference Proceedings, 3256(1). https://doi.org/10.1063/5.0267137

Sidorova, S.A., 2022. Safety of operation of support plates for the downstreams of hydraulic structures. Environmental Engineering, 1. Pp. 61-65.